P. Folegati, I. Makkonen, R. Ferragut, and M. J. Puska, Analysis of electron-positron momentum spectra of metallic alloys as supported by first-principles calculations, Physical Review B 75, 054201: 1-10 (2007).

Analysis of electron-positron momentum spectra of metallic alloys as supported by first-principles calculations

P. Folegati,[1,2,*] I. Makkonen,[2] R. Ferragut,[1] and M. J. Puska[2]

[1]*Dipartimento di Fisica e Centro L-NESS, Politecnico di Milano, Via Anzani 42, 22100 Como, Italy*
[2]*Laboratory of Physics, Helsinki University of Technology, P.O. Box 1100, FI-02015 TKK, Finland*

Electron-positron momentum distributions measured by the coincidence Doppler broadening method can be used in the chemical analysis of the annihilation environment, typically a vacancy-impurity complex in a solid. In the present work, we study possibilities for a quantitative analysis, i.e., for distinguishing the average numbers of different atomic species around the defect. First-principles electronic structure calculations self-consistently determining electron and positron densities and ion positions are performed for vacancy-solute complexes in Al-Cu, Al-Mg-Cu, and Al-Mg-Cu-Ag alloys. The ensuing simulated coincidence Doppler broadening spectra are compared with measured ones for defect identification. A linear fitting procedure, which uses the spectra for positrons trapped at vacancies in pure constituent metals as components, has previously been employed to find the relative percentages of different atomic species around the vacancy [A. Somoza *et al.* Phys. Rev. B **65**, 094107 (2002)]. We test the reliability of the procedure by the help of first-principles results for vacancy-solute complexes and vacancies in constituent metals.

PACS number(s): 78.70.Bj, 81.40.Cd

I. INTRODUCTION

In metallic alloys, solute-vacancy association is one of the basic processes controlling the precipitation phenomenon. Vacancies mediate transport of solute atoms and contribute to the stability of precipitates by reducing misfit stresses between them and the matrix material.[1] The precipitation process is technologically important, since it improves mechanical properties of a number of light Al- and Mg-based alloys widely used in the vehicle industry.

Positron annihilation spectroscopy is a well-recognized technique for investigating metallic alloys.[2,3] The kinetics of precipitation after mechanical and thermal treatments can be studied by positron lifetime spectroscopy, while the chemical environment of defects can be determined by coincidence Doppler broadening (CDB) spectroscopy. The use of CDB spectroscopy was extended to study the association of vacancies with solute atoms in metallic solid solutions only a few years ago,[4,5] but several CDB works regarding alloys have been published since then.[2,6–10]

CDB spectroscopy suit studying solute-vacancy complexes in Al alloys especially well because, as open-volume defects, they effectively trap positrons. Moreover, typical solute atoms, such as Cu, Zn, and Ag, have occupied *d* atom shells giving strong signals in the CDB momentum spectra in contrast to Al. The analysis of the CDB spectra is expected to give average concentrations of solute elements neighboring vacancies or vacancylike defects at matrix-precipitate interfaces. Somoza *et al.*[6] suggest to fit the CDB spectra with linear combinations of spectra measured for the matrix metal in the annealed state and those of elemental samples corresponding to all the constituents of the alloy after severe plastic deformation. The annealed matrix spectrum accounts for the annihilation of free positrons in bulk, whereas the deformed sample spectra take into account the effects of positron confinement at vacancies. Recently, the scheme has been revised by Ferragut[11] to take into account the nonsaturation

positron trapping by using the simultaneously measured positron lifetime spectra. The Appendix shows examples of the fitting scheme in the case of Al-Cu alloy samples.

In the present work, we study possibilities for quantitative analysis of solute-vacancy complexes in metallic alloys. More specifically, we choose the binary Al-Cu, ternary Al-Mg-Cu, and quarternary Al-Mg-Cu-Ag alloys and model the solute-vacancy complexes in them by first-principles electronic structure calculations. In the simulations, the ion positions are determined so that they are consistent with the electron density and also with the density of the trapped positron. The CDB spectra are also measured for the as-quenched and 1 min aged Al-(1.1 at %)Cu samples. The theoretical and experimental spectra are compared in order to find the most probable complexes present in the samples. The comparisons also emphasize the importance of fully relaxed ionic structures in calculating the CDB spectra.

We also study the reliability of the fitting procedure by Somoza *et al.* by comparing the first-principles results for different solute-vacancy complexes in binary, ternary, and quarternary alloys with those obtained by the linear combination of spectra calculated for vacancies in elemental deformed metals. A surprisingly good correspondence is found showing that the average numbers of solute atoms decorating the vacancy can be determined. However, in some cases, this may happen with the price of modifying the fraction of trapped positrons. Moreover, the distinction between adjacent atoms in the Periodic Table, e.g., Mg and Al, may be difficult.

The present paper is structured as follows. In Sec. II, we describe the defect models used in this work and in Sec. III, our computational approach. Results and discussion are presented in Sec. IV. Finally, we present our conclusions in Sec. V.

II. MODELING

In this work, we present the CDB data as ratio-difference (RD) spectra

$$\Delta(p) = \frac{\rho(p) - \rho_{\text{bulk}}(p)}{\rho_{\text{bulk}}(p)}, \qquad (1)$$

where $\rho(p)$ and $\rho_{\text{bulk}}(p)$ are the spectra corresponding to the vacancy defect and perfect bulk systems, respectively. This presentation is convenient, because partial annihilation in the bulk state (nonsaturation trapping) in the defect system does not affect the shape of the RD spectrum but only its amplitude.[12] Moreover, in the ratio, systematic theoretical errors in momentum density intensities cancel out.[13] When only one type of defect traps positrons, the trapping fraction F is the multiplicative factor needed to scale the defect spectrum (corresponding to saturation trapping) to coincide with the measured spectrum of the given defected system.[12] This fraction can be compared with the fraction obtained from positron lifetime measurements. However, usually in the case of alloys, only mean lifetimes can be extracted from the experiment and, therefore, F, in practice, acts as a free parameter in the fitting procedure.

We start to build up the model for vacancy-solute defects in Al alloys by considering deformed Al. This is because the positron data for the alloy resemble those of deformed Al in the sense of similar trapped positron lifetimes of 210–220 ps (Ref. 14), which are clearly shorter than the positron lifetime of 235 ps for as-quenched Al (Ref. 12). In the previous work,[12] we modeled a vacancy in deformed Al by moving the nearest-neighbor atoms of the vacancy inward and keeping the more distant atoms in their ideal Al lattice positions. The inward relaxation mimics the effects of strain due to dislocations with which vacancies are associated. In this work, we want to calculate from first principles the positions of the Al and solute atoms, and, therefore, the strain is taken into account by reducing the Al lattice constant. We choose the strain to reproduce the experimental positron lifetime value of 225 ± 1 ps for trapped positrons (Ref. 12). The strain needed is 4% with respect to the experimental lattice constant of 4.05 Å, resulting in a lattice constant of 3.89 Å. Also, the Doppler spectra for the vacancy in this strained Al is in a reasonable agreement with the experimental data for deformed Al (Ref. 12). Namely, the predicted curve has the correct shape and the scaling needed corresponds to the trapping fraction of 48%, which is comparable to the value of 64% deduced from the positron lifetime measurements. Apart from using the empirically determined lattice constant, we model the geometries of the vacancy-solute complexes from first principles. This means that the ionic structures of complexes are determined by minimizing the Hellman-Feynman forces due to the electronic structure and the localized positron state.[13]

Here, we want to remark that the determination of the amount of strain is actually based not only on the agreement of the theoretical and experimental positron lifetimes for the deformed Al; but also, for the unstrained case, our lifetimes agree well with the experimental ones (see Table I). Namely, for the bulk, we get the theoretical lifetime of 165 ps in good agreement with the experimental values of 153, 158, and 163 ps (Refs. 15–17, respectively) and our theoretical lifetime of 248 ps for the vacancy is consistent with the experimental ones of 235–248 ps (Refs. 12 and 17). For the

TABLE I. Theoretical, τ_{theor}, and experimental, τ_{exp}, positron lifetimes for elemental bulk metals and vacancies in them. Also, the lattice parameters a for the face-centered-cubic and the c/a ratios for the hexagonal-close-packed structures are shown. The non-strained lattice parameters are experimental values at room temperature (Ref. 18).

System	a (Å)	c/a	τ_{theor} (ps)	τ_{exp} (ps)
Al bulk,no strain	4.05		165	153,[a] 158,[b] 163[c]
Al vacancy			249	235,[d] 236,[a] 248[c]
Al bulk,strained	3.89		149	
Al vacancy,strained			226	225,[e] 240[f]
Cu bulk,no strain	3.61		103	109,[a] 112,[b] 119[g]
Cu vacancy			175	168,[a] 170,[h] 180[i]
Cu bulk, strained	3.52		95	
Cu vacancy, strained			160	170,[h] 178[e]
Mg bulk, no strain	3.21	1.62	230	219,[j] 225[k]
Mg bulk, strained	3.05	1.62	217	
Mg vacancy, strained			285	244[e]
Ag bulk, no strain	4.09		123	131,[l] 131[a]
Ag vacancy			196	207[a]
Ag bulk, strained	3.97		111	
Ag vacancy, strained			189	196[e]

[a]Reference 15.
[b]Reference 16.
[c]Reference 17.
[d]Reference 12.
[e]Reference 19.
[f]Reference 20.
[g]Reference 21.
[h]Reference 22.
[i]Reference 23.
[j]Reference 11.
[k]Reference 24.
[l]Reference 25.

vacancy-Cu complexes in Al, the experimental lifetimes are around 210 ps (Ref. 14) and our modeling, as will be discussed below in more detail, gives typically 210–220 ps.

In our tests for the fitting procedure by Somoza *et al.*, we also need the CDB spectra corresponding to vacancies in deformed Cu, Mg, and Ag. Similar to the Al case, their modeling is performed by using slightly reduced lattice constants. They are given in Table I along with the resulting positron lifetimes. The lifetimes are also compared with the measured ones. For Cu and Ag, the absolute values are typically too low, but the important relative differences between the vacancy and bulk lifetimes agree well with experiment. In the case of Mg, theory predicts a larger lifetime difference than the measured one.

Figure 1 shows the RD spectra relative to bulk Al calculated using the first-principles methods for vacancies in strained Al, Mg, Cu, and Ag metals. At high momenta, the Al and Mg RD spectra are rather similar, reflecting the reduction of annihilation with similar electron cores. The Al spectrum has a peak around 9×10^{-3} $m_0 c$ due to positron confinement.[12] In the Mg RD spectrum, there is a maximum at low momenta, reflecting the rather low electron density (and long positron lifetime) at the vacancy. In the Cu RD spectrum, the high level at high momenta is due to annihilation with Cu $3d$ electrons, whereas in the case of Ag, the peak at 10×10^{-3} $m_0 c$ originates from Ag $4d$ electrons. The difference between the Cu and Ag RD spectra reflects the
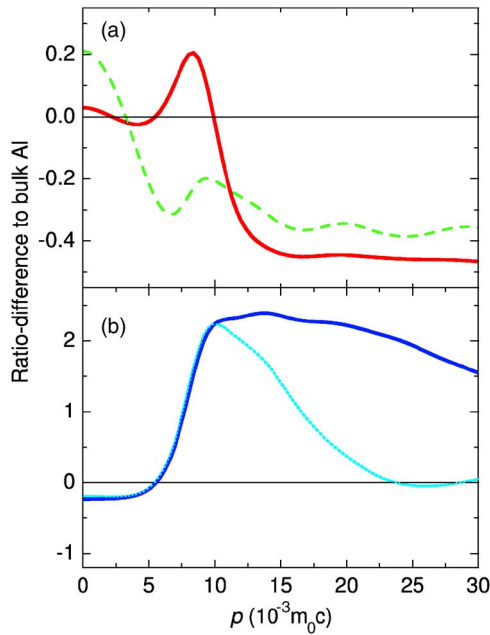
FIG. 1. (Color online) Calculated CDB RD spectra for vacancies in elemental strained metals. (a) The solid (red) line shows the result for the vacancy in strained Al and the dashed (green) line for the vacancy in strained Mg. (b) The solid (dark blue) line is the result for a vacancy in strained Cu and the dotted (light blue) line for the vacancy in strained Ag.

difference in the localization of the 3d and 4d electrons. The latter are more delocalized because 4d wave functions have to be orthogonal against 3d wave functions. The spectra in Fig. 1 are in good agreement with the experimental data presented in Ref. 26 and with those used in the experimental fitting procedure.[11]

III. COMPUTATIONAL METHOD

We model the defects in the face-centered-cubic Al, Cu, and Ag lattices using a cubic supercell of 32 atomic sites. For the hexagonal Mg, we use an orthorhombic supercell with 48 atomic sites. Valence electron densities are computed self-consistently in the framework of the local-density approximation (LDA) of the density-functional theory; the computations are carried out by employing the plane-wave code VASP (Refs. 27–29) with the projector augmented-wave (PAW) method[30] to account for the valence electron-ion core interaction. The first Brillouin zone of the superlattice is sampled using the $8 \times 8 \times 8$ Monkhorst-Pack **k**-point mesh.[31] A plane-wave cutoff of 342 eV is used when calculating the pseudovalence wave functions, in which the rapid oscillations near the ion cores are smeared off. The ionic structures of the vacancy-type defects are relaxed by taking into account, besides the forces on ions due to the electronic structure and ions, also the forces due to the localized positron.[13] Thereby, the electron and positron densities and ion positions depend on each other and they are solved in a self-consistent fashion. The PAW method also enables the postconstruction of all-electron valence wave functions which we use to accurately calculate the electron momentum densities.[13,32] The

cutoff equivalent to the momentum of the electron-positron pair of 70×10^{-3} m_0c is used when expanding all-electron valence wave functions in plane waves.

Using the PAW total charge density including the free atom core electrons, the positron potential is constructed within the LDA (Ref. 33) for electron-positron correlation effects. Then, the lowest-energy positron state is calculated on a three-dimensional real-space point grid.[13] The so-called conventional scheme, in which the localized positron density does not directly affect the average electron density, is used to describe trapped positrons. The annihilation rates of self-consistent all-electron valence states and those of the atomic core electron states are calculated within the LDA (Ref. 33) for the electron enhancement at the positron. These partial annihilation rates are used as weighting factors when calculating momentum densities of annihilating electron-positron pairs within the so-called state-dependent enhancement scheme.[34,35] For Al matrix systems, the momentum distributions corresponding to the valence electrons are obtained by the three-dimensional Fourier transformation on a cubic grid with the spacing of 0.67×10^{-3} m_0c and those for the core electrons on a dense radial grid using parametrized forms of the positron wave function.[34] The momentum densities for bulk Cu, Ag, and Mg and vacancies in them are calculated with accuracies similar to that for Al matrix. The ensuing three-dimensional momentum distributions are integrated over planes perpendicular to the [100] direction and convoluted with a Gaussian function with the full width at half maximum (FWHM) of 3.6×10^{-3} m_0c in order to simulate the experimental CDB spectra. In the case of asymmetric defects, we average over all possible orientations of the defect. For a complete description of the computational method, see Ref. 13. Calloni *et al.*[12] have previously used the same methodology (without the first-principles determination of the ionic relaxation) to study clean monovacancies in strained Al.

IV. RESULTS AND DISCUSSION

A. Ionic structures of vacancy-Cu complexes in the Al-Cu alloy and positron lifetime results

We have simulated vacancy-Cu complexes in the Al-Cu alloys by varying the number of Cu atoms, nearest neighbors to the vacancy, between 1 and 12. The resulting relaxed geometries and corresponding lifetimes are described in Table II. Up to four Cu atoms, it is reasonable to assume that the Cu atoms are on the same [100] plane around the Al vacancy, maximizing the Cu-Cu distances. This is because according to atomic probe field ion microscopy experiments, Cu tends to form platelets perpendicular to the ⟨100⟩ direction,[1,14,36] and also because according to our calculated total energies, these configurations are favored in contrast to more dense Cu clusters. However, as listed in Table II, in addition to these planar configurations, we have considered three Cu atoms as nearest neighbors to each other and four Cu atoms in a tetragonal configuration.

According to Table II, the larger the number of Cu atoms around the vacancy is, the stronger is the outward relaxation of the Cu atoms and the inward relaxation of the Al atoms.

TABLE II. Relaxations and positron lifetimes for vacancy-Cu complexes in the Al-Cu alloy. In the case of four Cu atoms, the planar and tetragonal configurations are considered. The ranges of relaxations are given for both Al and Cu nearest neighbors to the vacancy. The relaxations are relative to the ideal lattice positions and are given in percent of the bond length in the strained Al. A positive (negative) value denotes outward (inward) relaxation.

No. of Cu atoms	Relaxation, Al (%)	Relaxation, Cu (%)	Lifetime (ps)
0	+1.6		226
1	+0.5 to +1.5	+7.3	223
2	+0.3 to +0.8	+6.9	221
3[a]	−0.6 to +1.1	+5.6 to +6.2	218
3[b]	+1.1	+5.6 to +6.2	218
4[a]	−0.9	+5.9	216
4[c]	−2.7 to +0.4	+5.4 to +7.8	217
6	−3.3 to −2.1	+5.9 to +6.8	213
8	−5.7	+5.5	210
10	−9.9	+3.0 to +11.0	223
12		+7.4	235

[a]On the [100] plane.
[b]Nearest neighbors.
[c]Tetragonal.

For less than four Cu atoms, the Al atoms also tend to relax outward, but much less than the Cu atoms. The relatively long positron lifetime in the case of 12 Cu atoms is related to the strong outward relaxation, which increases the vacancy size compared with the other defects. The strong tendency of the Cu atoms to relax outward from the ideal Al lattice sites is in accordance with the effective medium theory by Jacobsen *et al.*,[37] which indicates that in metallic environments Cu atoms seek to a much higher electron density than Al atoms. The theory also explains why, according to our calculations, the change of the Cu atom configuration for a fixed number of Cu atoms does not significantly alter the open volume of the defect and the positron lifetime.

B. Comparing the experimental Al-Cu spectra with calculations for model systems

We proceed by analyzing the experimental CDB data for Al-Cu alloys using the previously described calculations for realistic model defects. Different simulated RD spectra are scaled separately, so that the least-squares method gives the best fit with those measured for the as-quenched and 1 min aged Al-(1.1 at %)Cu samples. The experimental procedure for obtaining these spectra is explained in the Appendix. Thus, we assume first that a single defect geometry can represent the whole defect distribution in the sample in an average manner. As explained above, the scaling means the fitting of the fraction F of positrons trapped at defects. Figure 2(a) shows the results for the as-quenched sample and simulated spectra with two, three, and four Cu atoms. The data for momenta up to $15 \times 10^{-3} m_0 c$ are included in the fitting. The best fit is obtained with three Cu atoms with the scaling
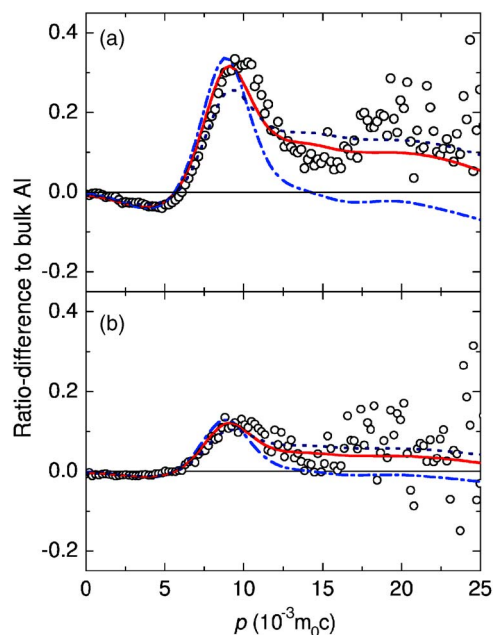

FIG. 2. (Color online) Experimental CDB spectrum (○) (RD to bulk Al) of (a) an as-quenched Al-(1.1 at %) Cu sample, and (b) the same sample aged 1 min at 150 °C. The dash-dotted (blue), solid (red), and dotted (black) lines show the best one-component fits obtained for vacancy-Cu defects with two, three, and four Cu atoms, respectively.

corresponding to the trapping fraction of 62%. The fits with two and four Cu atoms are clearly worse. Figure 3(d) below shows that taking the linear combination of the two and four -Cu-atom spectra with equal weights, we obtain a fit which practically coincides with the three-Cu-atom spectrum. Even the scaling needed remains the same. We can therefore conclude that the sample contains a distribution of vacancies with three Cu nearest neighbors on the average.

The above analysis using the first-principles-simulated RD curves agrees well with the analysis based on the linear combination of measured spectra for bulk Al and for deformed Al and Cu (see the Appendix). The fitting gives the Cu contribution of $(23 \pm 1.5)\%$, i.e., there are roughly three Cu atoms among the 12 nearest neighbors of the vacancy on the average. The trapping fraction is found to be $(73 \pm 1)\%$ which is slightly larger than the estimate based on the theoretical spectrum.

In the case of the 1 min aged sample, the experimental data points [Fig. 2(b)] are quite scattered because of the lower vacancy concentration and smaller trapping fraction. This complicates the fitting. However, as Fig. 2(b) shows, we get a reasonable fit also in this case when three are three or four Cu atoms next to the vacancy. These fits result in trapping fractions of 24% or 17%, respectively. These numbers should be contrasted with the experimental analysis of the Appendix indicating the Cu concentration of $(33 \pm 5)\%$, i.e., about four Cu atoms around the vacancy and the trapping fraction of $(18 \pm 1)\%$. However, because of the very scattered experimental data and low trapping fraction, it is difficult to draw accurate conclusions about the number of Cu atoms around the vacancy.
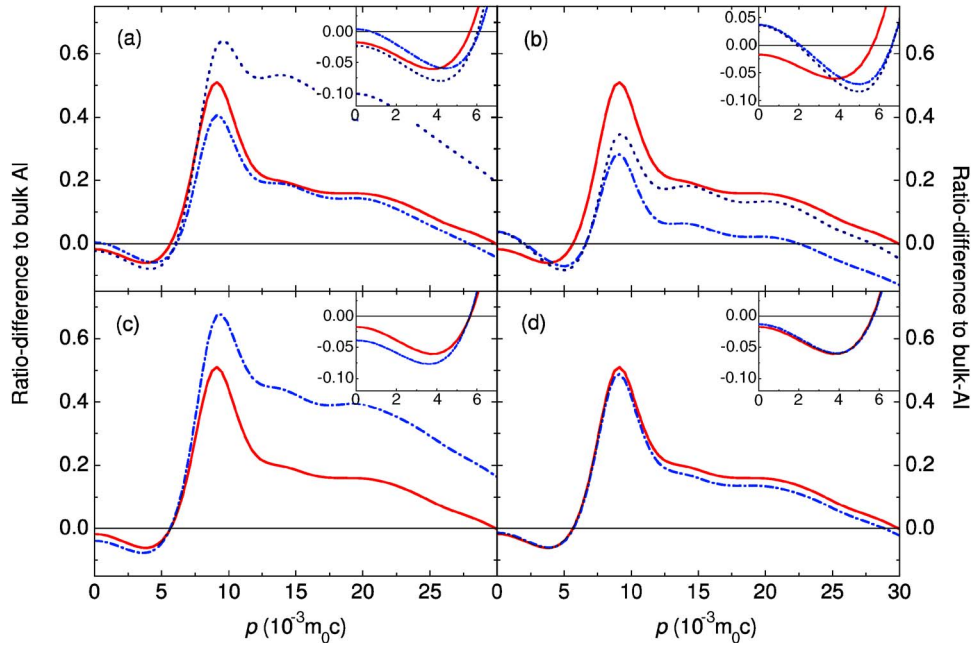
FIG. 3. (Color online) Influence of different approximations on the first-principles results for Al vacancies decorated with Cu atoms. In all panels, the solid (red) line shows the RD spectrum obtained for the Al vacancy surrounded by three Cu atoms on the [100] plane in the strained Al lattice including ionic relaxation due to the electronic structure and the localized positron state. (a) The dash-dotted (dark blue) and the dotted (blue) lines show the results corresponding to ideal (no relaxation) ion positions and for two and three Cu atoms, respectively. (b) The dash-dotted (dark blue) and the dotted (blue) lines correspond to the Al lattice without strain and to three and four Cu atoms, respectively. (c) The dash-dotted (dark blue) curve shows the result for three Cu atoms nearest neighbors to each other. (d) The dash-dotted (dark blue) curve corresponds to the fit using the linear combination of RD spectra for two and four Cu atoms with equal weights.

Now, we want to get an idea about the importance of different ingredients of our first-principles calculations on the simulated CDB RD spectra. Our reference system is the Al vacancy in the strained Al lattice decorated with three Cu atoms. Due to the good agreement with the experimental result shown in Fig. 2(a), this suits well as a representative test case. Figure 3(a) shows that ignoring the lattice relaxation relative to the ideal lattice positions increases the intensity at high momenta and decreases the relative intensity of the peak at around $p=9\times10^{-3}\ m_0c$. This change reflects the tendency of the Cu atoms to relax strongly outward (see Table II). The reduction of the number of Cu atoms to two would improve the agreement with experiment, but still the shape is worse than that of the fully relaxed three-Cu-atom case. The importance of using the strained Al lattice is emphasized in Fig. 3(b). Ignoring the strain increases the intensity at low momenta, indicating a too large open volume and a too long positron lifetime. The negative values at high momenta can be healed by increasing the number of Cu atoms to four, but this affects by worsening the relative intensity of the peak. Figure 3(c) shows that three Cu atoms nearest neighbors to each other result in a large intensity increase at high momenta with respect to the three Cu atoms on the same [100] plane. This is because the dense Cu cluster creates an open volume attracting the positron density and resulting in an increased annihilation with Cu $3d$ electrons. However, as discussed above, the planar configuration is favored against the dense one due to its lower calculated total energy and also due to the experimental findings.

C. Linear combinations of the elemental CDB spectra: Theory versus theory

The most important goal of the present work is to test the reliability of the linear-combination method adopted in the experimental data analysis (see the Appendix). For example, the RD spectrum $\Delta(p)$ for a vacancy-Cu complex in the Al-Cu alloy is fitted with the function

$$\Delta^{\text{fit}}(p) = F[C_{\text{Al}}\Delta^{\text{Vac}}_{\text{Al}}(p) + C_{\text{Cu}}\Delta^{\text{Vac}}_{\text{Cu}}(p)]$$
$$= F\left[\frac{N_{\text{Al}}}{12}\Delta^{\text{Vac}}_{\text{Al}}(p) + \frac{N_{\text{Cu}}}{12}\Delta^{\text{Vac}}_{\text{Cu}}(p)\right], \qquad (2)$$

where $\Delta^{\text{Vac}}_{\text{Al}}(p)$ and $\Delta^{\text{Vac}}_{\text{Cu}}(p)$ are the RD spectra for vacancies in strained (i.e., deformed) Al and Cu, respectively. F is the fraction of trapped positrons and N_{Al} and N_{Cu} are the numbers of Al and Cu nearest neighbors to the vacancy, respectively. The Al and Cu concentrations around the vacancy fulfill the constraint $C_{\text{Al}}+C_{\text{Cu}}=1$, so that there are only two free fitting parameters, e.g., F and C_{Cu}. Actually, F should be ideally equal to unity, but we will keep it as a fitting parameter in order to test the idea of the general fitting procedure. Figure 1 shows the theoretical elemental RD spectra we use in our fitting.

Instead of the experimental Al-Cu alloy data, we use here the RD spectra calculated from our first-principles results for Al vacancies decorated with Cu atoms and fit them using the similarly calculated RD spectra for vacancies in strained Al and Cu. Figure 4 shows the simulated RD curves for 2, 4, 8,
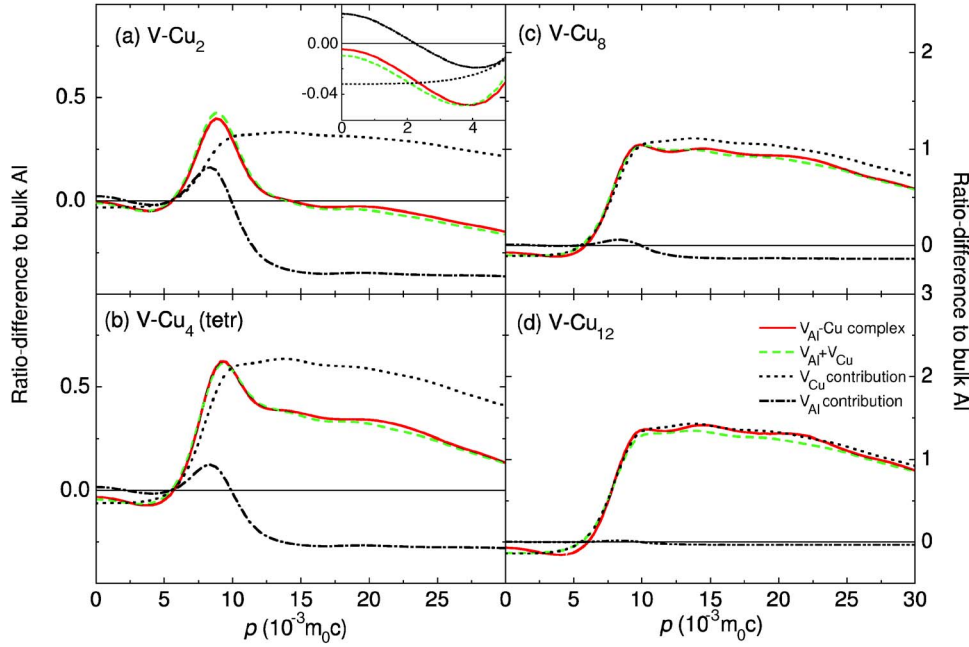
FIG. 4. (Color online) CDB RD spectra for vacancy-Cu complexes in Al-Cu alloys with (a) 2, (b) 4, (c) 8, and (d) 12 nearest neighbor Cu atoms. The tetragonal configuration is used in the case of four Cu atoms. The solid (red) curves give the results of the first-principles calculations. The dashed (green) curves are the linear combinations [Eq. (2)] of the RD spectra calculated for vacancies in strained Al and Cu. The dash-dotted and dotted curves show the Al and Cu contributions, respectively. The inset in (a) shows the magnified low-momentum region.

and 12 Cu atoms as the nearest neighbors to the vacancy. The linear combinations obtained with the least-squares method and their Al- and Cu-vacancy components are also shown. The momentum range of $(0-15) \times 10^{-3}$ m_0c is included in the fitting. As in the purely experimental analysis, the fits successfully reproduce the original curves. The decompositions show that the peak around 8×10^{-3} m_0c in the RD spectrum is due to the Al-vacancy component, and the Cu $3d$ derived electronic states are responsible for the rise of the intensity at high momenta. At the low-momentum region of $(0- \sim 7) \times 10^{-3}$ m_0c, the agreement between the simulated RD curve and the linear combination worsens with increasing number of Cu atoms surrounding the Al vacancy. This is due to the fact that the electron density at the vacancy in Cu is larger than that at the Al vacancy surrounded by Cu atoms.

More quantitatively, the fitting parameters F and C_{Cu} are given in Table III. The fitting seems to underestimate the Cu concentration consistently by around 10%. This rather good accuracy is obtained by the help of the reduction of the trapping fraction from its nominal value of unity. When the number of Cu atoms increases from 1 to 12, F decreases rather linearly from a value slightly less than unity to around 0.7. The reduced trapping fraction substitutes the annihilation with Cu by annihilation with bulk Al. This compensation is needed because the use of the Cu vacancy data would otherwise lead to too strong annihilation with Cu atoms due to the fact that the Cu lattice constant is smaller than that for Al. The reduced trapping fraction also decreases the contribution FC_{Al} of the Al-vacancy RD spectrum. This decrease is compensated by the increase of the ratio C_{Al}/C_{Cu}, but the effect of this "secondary" compensation is not strong and it decreases with the decreasing number of Cu atoms so that the ratio C_{Al}/C_{Cu} remains close to the correct one. Thus, the Cu concentration is estimated to be only 10% too small.

D. Vacancy-solute complexes in Al-Cu-Mg and Al-Cu-Mg-Ag alloys

Next, we want to investigate possibilities for quantitative analysis of vacancy-solute complexes when there are more than one type of solute atoms. As examples, we choose complexes in the technologically important ternary Al-Cu-Mg and quaternary Al-Cu-Mg-Ag alloys. The Al matrix around the defect complex is described by the strained Al lattice, the same as the above for the Al-Cu alloy. The ionic and electronic structures and the trapped positron density are calculated with the first-principles scheme.

TABLE III. Fitting the RD spectra calculated from the first-principles results for vacancy-Cu complexes in the Al-Cu alloy with the linear combination of calculated RD spectra for vacancies in strained Al and Cu. The fitting parameters, i.e., the number N_{Cu} of Cu atoms around the Al vacancy and the fraction of trapped positrons F, are defined in Eq. (2).

No. of Cu atoms in complex	N_{Cu}	F
1	1.00	0.967
2	1.80	0.924
3[a]	2.71	0.898
3[b]	3.84	0.912
4[a]	3.49	0.842
4[c]	3.67	0.868
6	5.54	0.811
8	7.38	0.758
10	9.05	0.762
12	10.66	0.671

[a]On the [100] plane.
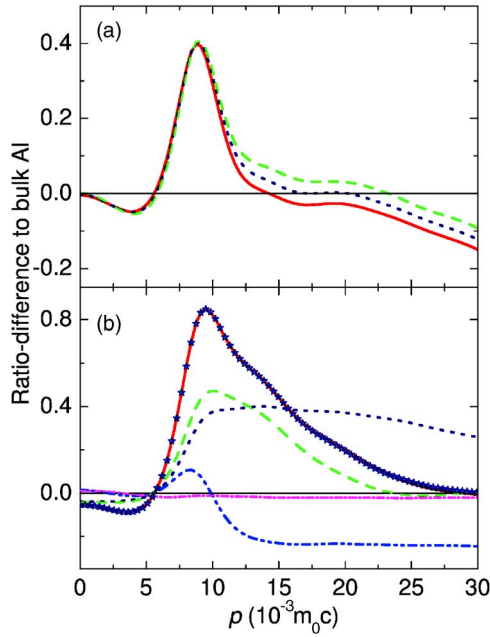[b]Nearest neighbors.
[c]Tetragonal.

FIG. 5. (Color online) (a) CDB RD spectra for vacancy-Cu-Mg complexes in Al-Cu-Mg alloys with two Cu and zero, one, and two Mg atoms denoted by solid (red), dotted (dark blue), and dashed (green) lines, respectively. (b) CDB RD spectrum for a vacancy surrounded by two Cu, two Mg, and two Ag atoms and the best linear-combination fit denoted by a solid (red) line and (blue) stars, respectively. The components of the fit, corresponding to the vacancies in strained Al, Cu, Mg, and Ag, are shown by dash-double-dotted (blue) line, dashed (dark blue) line, dash-dotted (pink) line, and long-dotted (green) lines, respectively.

Figure 5(a) shows the RD spectra of vacancy-Cu-Mg complexes when there are two Cu and zero, one, and two Mg atoms as nearest neighbors to the vacancy. All the solute atoms are on the same [100] plane with the two Cu atoms along a ⟨110⟩ direction. According to Fig. 1(b), one would expect that the primary effect of the increasing number of neighboring Mg atoms on the shape of the defect RD spectrum would be to linearly increase its intensity at low momenta. However, this is not the case. In Fig. 5(a), the effect of Mg at low momenta is negligible. At high momenta, where the annihilation with Cu $3d$ derived states and Al and Mg core states dominates in the defect spectrum, the effect of Mg is to increase positron annihilation with these states. First of all, Mg has a larger Wigner-Seitz radius than Al. This means that the open volume at the vacancy decreases with the increasing number of Mg atoms. The relaxation of Mg atoms in these systems is about −1.3% to −1.2% (minus sign denotes inward relaxation). The positron lifetime increase per Mg atom added is 2 ps. The effect of the decreased vacancy volume on the CDB RD spectrum is to increase core annihilation and decrease annihilation with low-momentum valence electrons at the vacancy. On the other hand, substituting Al by Mg decreases the electron density at the vacancy, which in turn increases the value of the RD spectrum at low momenta. This effect, however, is not strong enough to raise the peak at low momenta. This fact is also seen in results of the simulations in which there is only Al and Mg around the vacancy.

TABLE IV. Fitting the RD spectra calculated from the first-principles results for vacancy-Cu-Mg and vacancy-Cu-Mg-Ag complexes in the Al-Cu-Mg and Al-Cu-Mg-Ag alloys with the linear combination of calculated RD spectra for vacancies in strained Al, Cu, Mg, and Ag. The fitting is done by generalizing Eq. (2) to four components N_{Al}, N_{Cu}, N_{Mg}, and N_{Ag}, giving the number of Al, Cu, Mg, and Ag atoms around the vacancy, respectively. The fitting parameter F is related to the fraction of trapped positrons.

No. of Cu atoms	No. of Mg atoms	No. of Ag atoms	N_{Cu}	N_{Mg}	N_{Ag}	F
1	1		1.07	0.32		0.954
2	1		1.94	0.58		0.932
2	2		2.09	0.99		0.919
2	4		2.37	1.69		0.895
2	6		2.60	2.51		0.900
3	1		2.78	0.89		0.912
3[a]	1		2.87	0.66		0.906
3	3		3.16	1.40		0.894
4	4		4.10	2.19		0.868
5	2		4.79	1.52		0.882
2	2	2	2.08	0.71	2.63	0.963
2	4	2	2.60	1.40	1.77	0.980
4	2	2	3.66	1.12	2.35	0.975
3	1	1	3.10	0.53	0.81	0.994
3[a]	1	1	3.10	0.74	0.58	1.01
3	1	2	2.97	0.51	1.96	1.00
3[a]	1	2	2.93	0.55	2.05	1.01

[a]Different configurations of the nearest-neighbor solute atoms.

The possibility of quantitative identification of Mg at the vacancy-solute complexes is studied in Table IV, which shows the analysis results of the RD spectra calculated for several vacancy-Cu-Mg complexes. Up to four solute atoms, they are on the same [100] plane. A general trend is that Cu atoms tend relax strongly outward from the center of the vacancy up to ∼10% of the Al bond length, whereas Mg atoms tend to relax to slightly smaller amounts inward. The different behaviors reflect the trends in the Wigner-Seitz radii. The fitting with the spectra for vacancies in elemental strained metals is performed in the momentum range of $(0–15) \times 10^{-3}$ $m_0 c$. According to Table IV, the trapping fractions are closer to unity than in the case of vacancy-Cu complexes in Table III. This is because Cu has a smaller and Mg a larger Wigner-Seitz radius than Al, so that their effects tend to compensate each other. The analysis rather faithfully gives the correct number of Cu atoms, but the number of Mg atoms is clearly underestimated. This is because the Mg component in the fit, i.e., the RD spectrum for a vacancy in strained Mg, has a rather strong peak at low momenta due to the large Wigner-Seitz radius and the low electron density. In the denser Al lattice, Mg does not decrease the electron density to the portion deduced on the basis of the effect of the vacancy in Mg. Moreover, the effect on the RD spectrum at

low momenta is not necessarily a linear function of the number of Mg atoms as discussed above.

Table IV also shows the results for vacancy-Cu-Mg-Ag complexes. In these systems, the fitting procedure which is now extended up to 17×10^{-3} m_0c reproduces the correct trapping fraction extremely well. Also, N_{Cu} and N_{Ag} are described with reasonable accuracy. Ag can be separated because due to the $4d$ electrons its RD spectrum is in contrast to those of Mg and Al and has a strong intensity at high momenta, but, on the other hand, the Ag $4d$ contribution decays much faster than the Cu $3d$ contribution towards high momenta [see Fig. 1(b)]. For this reason, when analyzing systems with Ag, it is crucial to extend the momentum fitting region at least up to 17×10^{-3} m_0c in order to be able to differentiate between Ag and Cu. Again, the Mg content is underestimated, but the sum $N_{Al}+N_{Mg}$ is well described. Figure 5(b) shows, as a typical example, the spectrum and its decomposition for the vacancy complex with two Cu, two Mg, and two Ag atoms.

V. SUMMARY AND CONCLUSIONS

We have performed first-principles calculations for electronic structures, positron states, and ion positions at solute-vacancy complexes in metallic alloys Al-Cu, Al-Mg-Cu, and Al-Mg-Cu-Ag. The ensuing positron annihilation characteristics, positron lifetimes, and momentum distributions of annihilating electron-positron pairs have been calculated. Since the electron and positron densities as well as the ion positions depend on each other, they have to be determined in a self-consistent fashion. We have shown that this step is required in order to obtain the annihilation characteristics consistent with the experimental ones.

The calculated ratio-difference curves of the Doppler broadening spectra are compared with the measured ones in order to quantitatively identify the vacancy-solute defects, i.e., to determine the average numbers of different solute atoms around the vacancies. An experimental spectrum can be interpreted in terms of a spectrum calculated for a certain defect configuration or by a linear combination of spectra for two or more defect configurations.

By the help of the first-principles results for vacancy-solute complexes and vacancies in constituent metals, we have tested the linear fitting procedure suggested by Somoza *et al.* to find the percentages of different atomic species around the vacancies. With the Al-Cu, Al-Mg-Cu, and Al-Mg-Cu-Ag alloys as test cases, we have shown that the linear combination can resolve the average number of solute atoms whose electronic structures clearly differ from those of the matrix and other solute atoms (such as Cu and Ag in our tests). Typically, an accuracy better than 0.5–1.0 atoms from the 12 nearest neighbors can be achieved. However, adjacent atoms of the Periodic Table having similar core electron structures (such as Mg and Al) cannot be distinguished.

In our test cases, the most important momentum region for the linear-combination fits is above $\sim 7 \times 10^{-3}$ m_0c. In this region, the behavior of the electron wave functions near the ion cores is important, leading to the distinction of the different atomic species. The lower momenta are dominated by free-electron-type behavior, which depends mainly on the average valence electron density seen by the positron. The introduction of solute atoms does not introduce changes such as new covalent bonds which would affect the above division to free-electron and atomic-specific regions. However, in order to mimic this division in linear-combination fits in a reasonable manner, it is important to use the vacancy spectra, and not the bulk spectra of solute metals as components.

The linear fitting procedure works well, besides due to the reasons mentioned above, also due to compensating effects affecting the positron annihilation rates with different ion cores. The rates depend on open space seen by the positron, and this may differ between the matrix and solute metal lattices. Compensation may occur when there are two or more different types of solute atoms around the vacancy. Compensation may also occur by underestimating or overestimating the fraction of trapped positrons if the fraction is kept as a free parameter in the fit. Therefore, comparing the fitted trapping fraction with that obtained by using the positron lifetime measurements is a valuable tool to check the consistency of the linear fitting procedure.

ACKNOWLEDGMENTS

APPENDIX: DETAILS OF THE EXPERIMENTS AND THE EXPERIMENTAL FITTING PROCEDURE

The experimental data presented below refer to two pairs of samples of a well-homogenized laboratory alloy, obtained by melting commercially pure elements. The nominal composition of the alloy was Al-(1.1 at %)Cu. All samples were solution treated by holding at 525 °C for 1 h and were then water quenched at room temperature. One pair of samples was immediately mounted in the standard sandwich configuration with a ^{22}Na positron source (about 2×10^5 Bq) sealed between Kapton foils and brought at liquid nitrogen temperature within less than a minute since quenching. The second pair was aged in oil bath for 1 min at 150 °C, then quenched again at room temperature, mounted with the positron source, and cooled as described for the other pair. All lifetime and CDB measurements were taken simultaneously at liquid nitrogen temperature; setups and procedures were already described in Ref. 12. The momentum resolution was 3.69×10^{-3} m_0c (FWHM). The time resolution of the lifetime apparatus was 250 ps (FWHM).

The analysis of the lifetime spectrum was carried out by means of the POSITRONFIT program[38] in a single component
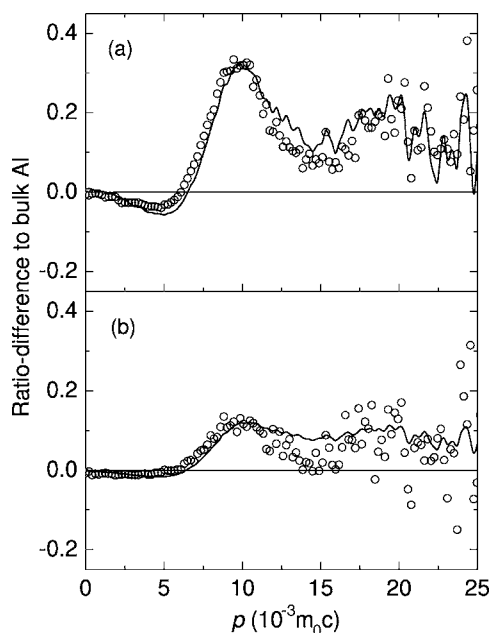
FIG. 6. Results of CDB measurements (markers) for (a) Al-(1.1 at %)Cu alloy measured after quenching and (b) after 1 min aging at 150 °C. The solid lines show the empirical fitting curves.

after subtraction of 12.5% source component. The CDB empirical analysis was performed by applying a modified version of the linear combination procedure suggested by Somoza *et al.*[6]

TABLE V. Empirical fitting coefficients F, C_{Al}, and C_{Cu} and the mean positron lifetimes τ for the Al-(1.1 at %)Cu alloy after quenching and after 1 min aging at 150 °C.

Sample	F (%)	C_{Al} (%)	C_{Cu} (%)	τ (ps)
As quenched	73±1	77±1.5	23±1.5	196±1
Aged 1 min at 150 °C	18±1	67±5	33±5	169±1

In the present version, the CDB spectrum ρ was fitted with a revised version of a linear combination (see Ref. [11]) of three reference spectra, ρ_{Al}^{bulk}, ρ_{Al}^{v}, ρ_{Cu}^{v}, measured, respectively, for (a) bulk annealed Al (no positron trapping), (b) deformed Al (100% positron trapping, after correction for the contribution of free positrons), (c) deformed Cu (100% positron trapping, after correction for the contribution of free positrons). The linear-combination can be written in the form

$$\rho = (1 - F)\rho_{Al}^{bulk} + F(C_{Al}\rho_{Al}^{v} + C_{Cu}\rho_{Cu}^{v}), \tag{A1}$$

where F is the proposed estimate of the positron fraction trapped at vacancy-solute clusters and C_{Al} and C_{Cu} are the proposed estimates of the fractional atomic concentrations in contact with the vacancy.

The same experimental data as in Fig. 2 and the empirical fitting curve [Eq. (A1)] are shown in Fig. 6 versus the modulus of the momentum component. The numerical results of the CDB analysis and the mean positron lifetimes are reported in Table V.

*Electronic mail: paola.folegati@polimi.it

[1] S. P. Ringer and K. Hono, Mater. Charact. **44**, 101 (2000).

[2] A. Dupasquier, G. Kögel, and A. Somoza, Acta Mater. **52**, 4707 (2004).

[3] A. Dupasquier, P. Folegati, N. de Diego, and A. Somoza, J. Phys.: Condens. Matter **10**, 10409 (1998).

[4] M. Biasini, G. Ferro, P. Folegati, and G. Riontino, Phys. Rev. B **63**, 092202 (2001).

[5] Y. Nagai, Z. Tang, and M. Hasegawa, Radiat. Phys. Chem. **58**, 737 (2000).

[6] A. Somoza, M. P. Petkov, K. G. Lynn, and A. Dupasquier, Phys. Rev. B **65**, 094107 (2002).

[7] A. Dupasquier, A. Somoza, R. N. Lumley, and I. J. Polmear, in *Proceedings of the Ninth International Conference on Aluminum Alloys*, edited by J. F. Nie, A. J. Morton, and B. C. Muddee (Institute of Materials Engineering Australasia, Melbourne, 2004), pp. 1135–1140.

[8] Y. Nagai, M. Murayama, Z. Tang, T. Nonaka, K. Hono, and M. Hasegawa, Acta Mater. **49**, 913 (2001).

[9] Y. Nagai, T. Honma, Z. Tang, K. Hono, and M. Hasegawa, Philos. Mag. A **82**, 1559 (2002).

[10] Y. Nagai, K. Hono, S. Yanagita, T. Honma, and M. Hasegawa, in *Proceedings of the Ninth International Conference on Aluminum Alloys*, edited by J. F. Nie, A. J. Morton, and B. C. Muddee (Institute of Materials Engineering Australasia, Melbourne,

2004), pp. 287–292.

[11] R. Ferragut (unpublished).

[12] A. Calloni, A. Dupasquier, R. Ferragut, P. Folegati, M. M. Iglesias, I. Makkonen, and M. J. Puska, Phys. Rev. B **72**, 054112 (2005).

[13] I. Makkonen, M. Hakala, and M. J. Puska, Phys. Rev. B **73**, 035103 (2006).

[14] R. K. W. Marceau, R. Ferragut, A. Dupasquier, M. M. Iglesias, and S. P. Ringer, Mater. Sci. Forum **519-521**, 197 (2006).

[15] K. Petters, Diploma work, Martin-Luther Universität Halle-Wittenberg, 1998.

[16] T. E. M. Staab, B. Somieski, and R. Krause-Rehberg, Nucl. Instrum. Methods Phys. Res. A **381**, 141 (1996).

[17] H. E. Schaefer, R. Gugelmeier, M. Schmolz, and A. Seeger, in *Proceedings of the Eighth International Conference on Vacancies and Interstitials in Metals and Alloys*, edited by C. Ambromeit and H. Wollenberger (Trans Tech, Aedermannsdorf, 1986).

[18] C. Kittel, *Introduction to Solid State Physics*, 7th ed. (J. Wiley and Sons, New York, 1996).

[19] P. Folegati, A. Dupasquier, R. Ferragut, M. M. Iglesias, I. Makkonen, and M. J. Puska, Phys. Status Solidi C (to be published).

[20] T. E. M. Staab, E. Zschech, and R. Krause-Rehberg, J. Mater. Sci. **35**, 4667 (2000).

[21] L. C. Smedskjaer, M. J. Fluss, D. G. Legnini, M. K. Chason, and

R. W. Siegel, J. Phys. F: Met. Phys. **7**, 1715 (1977).

[22] T. E. M. Staab, R. Krause-Rehberg, and B. Kieback, J. Mater. Sci. **34**, 3833 (1999).

[23] G. Dlubek, in *Proceedings of the Fourth International Conference on Age-Hardenable Aluminium Alloys*, edited by I. Kovacs and J. Lendvai [Mater. Sci. Forum, **13/14**, 11 (1987)].

[24] P. Hautojärvi, J. Johansson, A. Vehanen, J. Yli-Kauppila, J. Hillairet, and P. Tsanetakis, Appl. Phys. A: Solids Surf. **27**, 49 (1982).

[25] H. E. Schaefer, W. Stuck, F. Banhart, and W. Bauer, in *Proceedings of the Eighth International Conference on Vacancies and Interstitials in Metals and Alloys*, edited by C. Ambromeit and H. Wollenberger (Trans Tech, Aedermannsdorf, 1986).

[26] R. Ferragut, A. Dupasquier, M. M. Iglesias, C. E. Macchi, A. Somoza, and I. J. Polmear, Mater. Sci. Forum **519-512**, 309 (2006).

[27] G. Kresse and J. Furthmüller, Comput. Mater. Sci. **6**, 15 (1996).

[28] G. Kresse and J. Furthmüller, Phys. Rev. B **54**, 11169 (1996).

[29] G. Kresse and D. Joubert, Phys. Rev. B **59**, 1758 (1999).

[30] P. E. Blöchl, Phys. Rev. B **50**, 17953 (1994).

[31] H. J. Monkhorst and J. D. Pack, Phys. Rev. B **13**, 5188 (1976).

[32] I. Makkonen, M. Hakala, and M. J. Puska, J. Phys. Chem. Solids **66**, 1128 (2005).

[33] E. Boroński and R. M. Nieminen, Phys. Rev. B **34**, 3820 (1986).

[34] M. Alatalo, B. Barbiellini, M. Hakala, H. Kauppinen, T. Korhonen, M. J. Puska, K. Saarinen, P. Hautojärvi, and R. M. Nieminen, Phys. Rev. B **54**, 2397 (1996).

[35] B. Barbiellini, M. Hakala, M. J. Puska, R. M. Nieminen, and A. A. Manuel, Phys. Rev. B **56**, 7136 (1997).

[36] K. Hono, Acta Mater. **47**, 3127 (1999).

[37] K. W. Jacobsen, J. K. Norskov, and M. J. Puska, Phys. Rev. B **35**, 7423 (1987).

[38] P. Kirkegaard, N. J. Pedersen, and M. Eldrup, *PATFIT-88: A Data-Processing System for Positron Annihilation Spectra on Mainframe and Personal Computers* (Risø National Laboratory, Roskilde, 1989).